

Fully microscopic shell-model calculations with realistic effective hamiltonians

L. Coraggio¹, A. Covello^{1,2}, A. Gargano¹, N. Itaco^{1,2}, and T. T. S. Kuo³

¹Istituto Nazionale di Fisica Nucleare and ² Dipartimento di Scienze Fisiche, Università di Napoli Federico II,

Complesso Universitario di Monte S. Angelo, Via Cintia - I-80126 Napoli, Italy

³Department of Physics, SUNY, Stony Brook, New York 11794, USA

E-mail: luigi.coraggio@na.infn.it

Abstract. The advent of nucleon-nucleon potentials derived from chiral perturbation theory, as well as the so-called $V_{\text{low-}k}$ approach to the renormalization of the strong short-range repulsion contained in the potentials, have brought renewed interest in realistic shell-model calculations. Here we focus on calculations where a fully microscopic approach is adopted. No phenomenological input is needed in these calculations, because single-particle energies, matrix elements of the two-body interaction, and matrix elements of the electromagnetic multipole operators are derived theoretically. This has been done within the framework of the time-dependent degenerate linked-diagram perturbation theory. We present results for some nuclei in different mass regions. These evidence the ability of realistic effective hamiltonians to provide an accurate description of nuclear structure properties.

1. Introduction

The main problem with nuclear shell-model calculations is the choice of the input ingredients, namely the single-particle (SP) energies and the matrix elements of the residual two-body interaction (TBME).

A phenomenological approach to this problem, which has been successfully applied in different mass regions, is to treat these quantities as parameters to be least-squares fitted to a chosen set of experimental data (see for instance [1]).

A more fundamental approach is to start from the free nucleon-nucleon (NN) potential and derive an effective shell-model hamiltonian in the framework of a many-body theory (see for instance [2, 3]). Usually, the SP energies are taken from experiment and only the TBME are retained from the theoretical effective hamiltonian. This approach, that started with the pioneering work of Kuo and Brown [4] for the sd -shell region, in the last decade has proven to be a viable way to provide an accurate description of nuclear structure properties. A review of some results may be found in Ref. [2].

However, the advances in computational power and the refinement of the time-dependent degenerate linked-diagram perturbation theory [2] to derive the shell-model effective hamiltonian have paved the way to a fully microscopic approach to the nuclear shell-model, that is to employ both SP energies and TBME derived from theory.

Here, we present some examples of fully-microscopic shell-model calculations we have performed in different mass regions [5–8], to verify the practical value of this approach.

In the following section, we outline the perturbative approach to the derivation of a realistic shell-model hamiltonian. In Section III, we present results of shell-model calculations for heavy carbon and oxygen isotopes, *pf*-shell nuclei, and $N = 82$ isotones. A short summary is given in the last section.

2. Outline of calculations

We calculate the two-body shell-model effective hamiltonian within the framework of the time-dependent degenerate linked-diagram expansion [2].

This means that we describe the wave function of a nucleus with two valence nucleons as a two-nucleon state whose energy is calculated taking into account the interaction of the two valence nucleons with the closed core perturbatively. To this end, an auxiliary one-body potential U is introduced to break up the hamiltonian as the sum of an unperturbed term H_0 , which describes the independent motion of the nucleons, and a residual interaction H_1 :

$$H = \sum_{i=1}^A \frac{p_i^2}{2m} + \sum_{i<j} V_{NN}^{ij} = T + V_{NN} = (T + U) + (V_{NN} - U) = H_0 + H_1 \quad .$$

The effective hamiltonian H_{eff} is expressed through the Kuo-Lee-Ratcliff folded-diagram expansion in terms of the vertex function \hat{Q} -box, which is composed of irreducible valence-linked diagrams [2]. We include in the \hat{Q} -box one- and two-body Goldstone diagrams through third order in H_1 . The folded-diagram series is summed up to all orders using the Lee-Suzuki iteration method [9].

H_{eff} contains one-body contributions, whose collection is the so-called \hat{S} -box [10]. In realistic shell-model calculations it is customary to use a subtraction procedure, so that only the two-body terms of H_{eff} , which make up the effective interaction V_{eff} , are retained while the SP energies are taken from experiment [11]. In fully microscopic shell-model calculations, we adopt a different approach employing SP energies obtained from the \hat{S} -box calculation. In this regard, it is worth pointing out that, owing to the presence of the $-U$ term in H_1 , self-consistency correction diagrams arise in the \hat{Q} -box. In our calculation we use the harmonic oscillator potential, and take into account all self-consistency correction diagrams up to third order.

Let us now focus our attention on the input interaction V_{NN} . It would of course be very desirable to use directly a realistic NN potential that reproduces the two-body scattering data and deuteron properties with high precision. However, to perform nuclear structure calculations with realistic NN potentials in a perturbative framework, one has first to deal with the strong repulsive behavior of such potentials in the high-momentum regime. An advantageous method to renormalize the bare NN interaction has been proposed in [12]. It consists in deriving from V_{NN} a low-momentum potential $V_{\text{low-k}}$ defined within a cutoff momentum Λ by way of a similarity transformation. This is a smooth potential which preserves exactly the onshell properties of the original V_{NN} and is suitable for being used directly in nuclear structure calculations [2].

We have derived from the high-precision CD-Bonn NN potential [13] a $V_{\text{low-k}}$ corresponding to a value of the cutoff $\Lambda = 2.6 \text{ fm}^{-1}$, and this potential has been employed to derive shell-model effective hamiltonians both for *pf*-shell nuclei and $N = 82$ isotones.

A new and alternative approach to the renormalization of NN potential with a repulsive short-range component, such as the CD-Bonn one, is to employ a low-momentum realistic interaction derived from chiral perturbation theory at next-to-next-to-next-to-leading order. This is the so-called $N^3\text{LOW}$ NN potential [6] with a sharp momentum cutoff at 2.1 fm^{-1} , which we have employed to derive shell-model hamiltonians for heavy carbon and oxygen isotopes.

3. Results and comparison with experiment

In this section, we show and discuss results of shell-model calculations we have performed for nuclei with mass ranging from $A = 16$ to $A = 154$. Let us start with the isotopic chain of the heavy carbon isotopes for which we have used an effective shell-model hamiltonian derived from the $N^3\text{LOW}$ potential, with ^{14}C considered as an inert core [8].

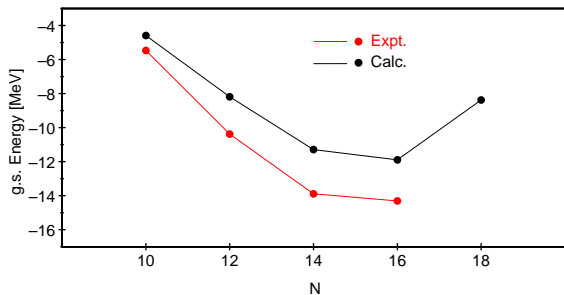


Figure 1. (Color online) Experimental [14, 15] and calculated ground-state energies for carbon isotopes from $A = 16$ to 24. N is the number of neutrons. See text for details.

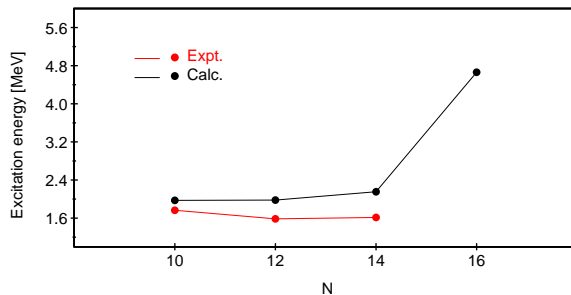


Figure 2. (Color online) Experimental [16, 17] and calculated excitation energies of the yrast $J^\pi = 2^+$ states for carbon isotopes from $A = 16$ to 22. N is the number of neutrons.

This is a challenging subject, because in a recent Letter [15] Tanaka *et al.* have reported on the observation of the neutron dripline for the carbon isotopes, which has been located at ^{22}C . This nucleus may be considered the heaviest Borromean nucleus ever observed [18] and it may be seen as composed of three parts: two neutrons plus ^{20}C . These three pieces must all be present in order to obtain a bound nucleus, as is proved by the particle instability of ^{21}C .

In Fig. 1 the calculated ground-state (g.s.) energies of the even-mass isotopes (continuous black line) relative to ^{14}C are compared with the experimental ones (continuous red line) [14]. The experimental behavior is well reproduced, in particular our results confirm that ^{22}C is the last bound isotope; its calculated two-neutron separation energy S_{2n} is 601 keV to be compared with the evaluation of 420 keV [14]. Moreover, our calculations predict that ^{21}C is unstable against one-neutron decay, the theoretical S_n being -1.6 MeV. Therefore, our results fit the picture of ^{22}C as a Borromean nucleus.

In Fig. 2 we report the experimental excitation energies of the yrast 2^+ states as a function of N and compare them with our calculated values. It can be seen that the observed energies are nicely reproduced. We also report our predicted excitation energy, 4.661 MeV, for the unbound $J^\pi = 2_1^+$ state in ^{22}C .

A similar calculation, starting also from the $N^3\text{LOW}$ potential, has been performed for the chain of the oxygen isotopes, where ^{16}O has been considered as the inert core.

In Fig. 3 the calculated g.s. energies of even-mass isotopes (continuous black line) relative to ^{16}O are compared with the experimental ones (continuous red line) [14]. From the inspection of Fig. 3, it can be seen that our calculations overestimate the experimental data. It is worth noting that this discrepancy may be “healed” by upshifting the calculated SP spectrum so as to reproduce the experimental g.s. energy of ^{17}O relative to ^{16}O . The results obtained with this upshift (427 keV) are reported in Fig. 3 by the black dashed line, and we see that the neutron dripline is located at ^{24}O . The need for this shift can be probably traced to the lack in our hamiltonian of a three-body force in addition to the $N^3\text{LOW}$ two-body potential [6].

In Fig. 4 the experimental and calculated excitation energies of the yrast 2^+ states are reported as a function of A . It can be seen that the observed energies, as well as the subshell closures at $N = 14$ and 16, are nicely reproduced. It should be noted that experimentally the $N = 14$ subshell closure disappears when moving from oxygen to carbon isotopes [20]. We see

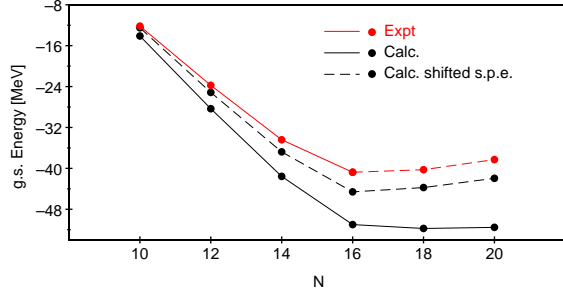


Figure 3. (Color online) Experimental [14] and calculated ground-state energies for oxygen isotopes from $A = 18$ to 28. N is the number of neutrons. The red dashed line refers to (non-experimental) estimated values [14]. See text for details.

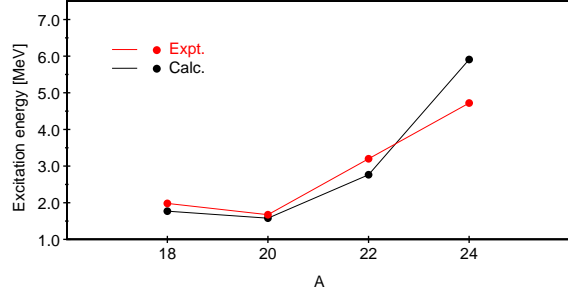


Figure 4. (Color online) Experimental [19] and calculated excitation energies of the yrast $J^\pi = 2^+$ states for oxygen isotopes from $A = 18$ to 24. N is the number of neutrons.

that this is correctly reproduced by our calculations when comparing the results shown in Figs. 2 and 4.

As mentioned in Section II, we have also performed calculations starting from a $V_{\text{low-}k}$ derived from the CD-Bonn potential. Let us now examine the region of pf -shell nuclei which have been studied deriving an effective hamiltonian for valence nucleons interacting in the four pf orbitals outside doubly-closed ^{40}Ca .

In Fig. 5 we have plotted the calculated (continuous black line) and experimental (continuous red line) g.s. energies per valence neutron of even-mass calcium isotopes, relative to ^{40}Ca , as a function of A . As in the case of the oxygen isotopes, our calculations overestimate the experimental data, and this may again be traced to the lack of the inclusion of a three-body force that could correct the calculated SP spectrum. In fact, if we upshift the latter so as to reproduce the experimental ^{41}Ca binding energy respect to ^{40}Ca , our results are upshifted by about 1.6 MeV (black dashed line), thus leading to good agreement with the experimental data along the whole isotopic chain.

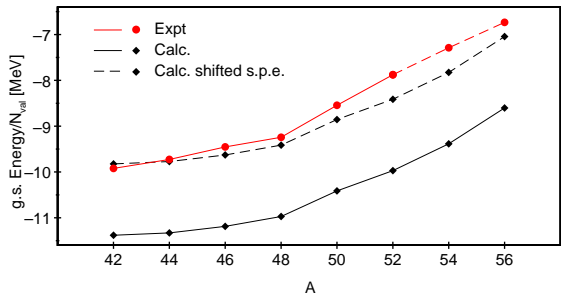


Figure 5. (Color online) Experimental [14] and calculated ground-state energies per valence neutron for calcium isotopes from $A = 42$ to 56. N_{val} is the number of valence neutrons. See text for details.

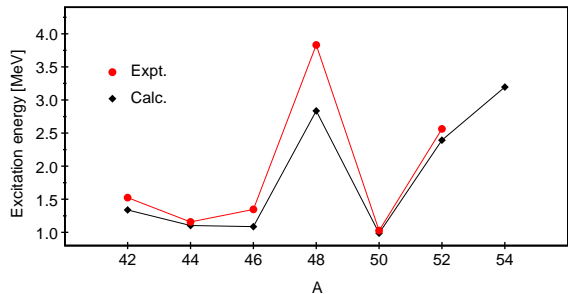


Figure 6. (Color online) Experimental [19] and calculated excitation energies of the yrast $J^\pi = 2^+$ states for calcium isotopes from $A = 42$ to 54.

The good quality of our effective interaction for calcium isotopes is further confirmed by the inspection of Fig. 6, where the experimental and calculated excitation energies of the yrast 2^+ states are reported as a function of A . It can be seen that our calculations reproduce nicely the

observed energies, apart from a quenching of the $N = 28$ shell closure. It should be mentioned that in the calculations for Ca isotopes reported in Ref. [21], we have employed an empirical set of SP energies, whose main difference respect to the theoretical one is the larger energy gap between the $p_{3/2}$ and $f_{7/2}$ levels, that is mainly responsible for the excitation energy of $J^\pi = 2^+$ state in ^{48}Ca .

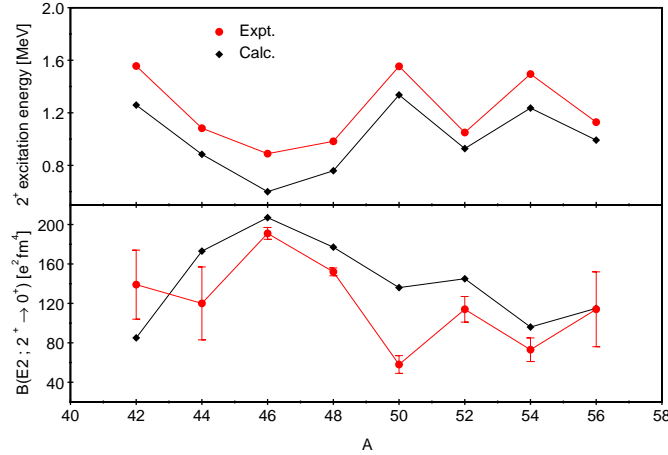


Figure 7. (Color online) Experimental [19] and calculated excitation energies of the yrast $J^\pi = 2^+$ states and their relative $B(E2; 2_1^+ \rightarrow 0_1^+)$ transition rates for titanium isotopes from $A = 42$ to 56.

In order to prove the reliability of our calculations when dealing with valence proton-neutron systems, in Fig. 7 we have plotted the excitation energy of the yrast 2^+ state as a function of A in even-mass Ti isotopes. In the same figure we also report the $B(E2; 2_1^+ \rightarrow 0_1^+)$ transition rates, calculated employing an effective operator obtained at third order in perturbation theory, consistently with the derivation of H_{eff} . A relevant result is that the theory reproduces the staggering of the transition rates for the heavy isotopes. Note that the enhancement of the $B(E2)$ transition rate in ^{56}Ti seems to suggest a softening of the $N = 34$ subshell closure [22].

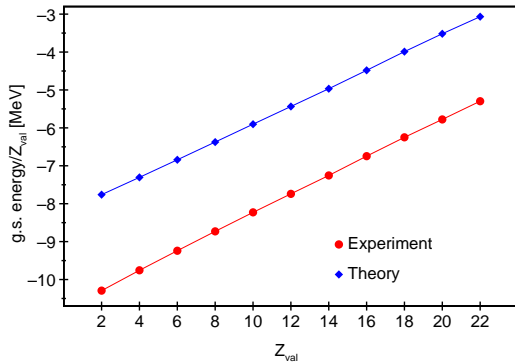


Figure 8. (Color online) Experimental and calculated ground-state energies per valence proton for $N = 82$ isotones from $A = 134$ to 154. Z_{val} is the number of valence protons.

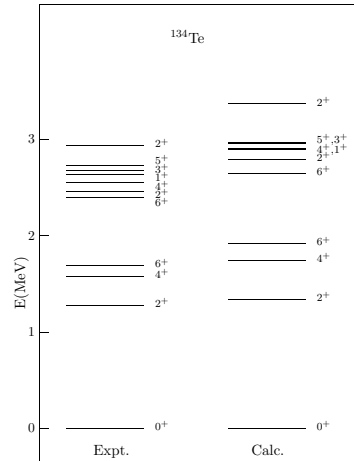


Figure 9. Experimental and calculated ^{134}Te spectra.

Finally, we present some selected results obtained for the even-mass $N = 82$ isotones starting from a $V_{\text{low-k}}$ derived from the CD-Bonn potential [7].

In Fig. 8, we show the calculated and experimental [14] g.s. energies (relative to the ^{132}Sn core) per valence proton of even-mass isotones as a function of the number of valence particles Z_{val} . We see that the experimental and theoretical curves are practically straight lines having the same slope while being about 2.4 MeV apart. This discrepancy is essentially the same as that existing between the theoretical and experimental g.s. energies of ^{133}Sb . This confirms the reliability of our SP spacings and TBME, since the pattern of the theoretical curve depends only on these quantities.

A strong test for the effective hamiltonian is given by the calculation of the energy spectrum of ^{134}Te , since the theory of the effective interaction is tailored for systems with two valence nucleons. In Fig. 9, the experimental [19] and calculated ^{134}Te spectra are reported up to 3.5 MeV excitation energy. It is worth mentioning that the quality of the results is comparable to that obtained in our previous calculations where the SP energies have been taken from experiment [23].

4. Concluding remarks

We have presented some selected results of shell-model studies within the framework of a fully microscopic approach. This means that, starting from a realistic NN potential, an effective hamiltonian has been derived by way of perturbation theory and then employed in our shell-model calculations without use of any adjustable parameter.

When compared with experiment, the quality of our results shows the practical value of this approach, as they reproduce correctly saturation and shell-closure properties, as well as many different spectroscopic features of the nuclear structure.

In our opinion these calculations, that make use of both single-particle energies and two-body matrix elements derived from the theory, may provide reliable predictions that do not depend on any phenomenological input.

References

- [1] Brown B A 2001 *Prog. Part. Nucl. Phys.* **47** 517
- [2] Coraggio L, Covello A, Gargano A, Itaco N and Kuo T T S 2009 *Prog. Part. Nucl. Phys.* **62** 135
- [3] Hjorth-Jensen M, Kuo T T S and Osnes E 1995 *Phys. Rep.* **261** 125
- [4] Kuo T T S and Brown G E 1966 *Nucl. Phys.* **85** 40
- [5] Coraggio L and Itaco N 2005 *Phys. Lett. B* **616** 43
- [6] Coraggio L, Covello A, Gargano A, Itaco N, Kuo T T S, Entem D R and Machleidt R 2007 *Phys. Rev. C* **75** 024311
- [7] Coraggio L, Covello A, Gargano A, Itaco N and Kuo T T S 2009 *Phys. Rev. C* **80** 044320
- [8] Coraggio L, Covello A, Gargano A and Itaco N 2010 *Phys. Rev. C* **81** 064303
- [9] Suzuki K and Lee S Y 1980 *Prog. Theor. Phys.* **64** 2091
- [10] Shurpin J, Kuo T T S and Strottman D 1983 *Nucl. Phys. A* **408** 310
- [11] Covello A, Coraggio L, Gargano A and Itaco N 2001 *Acta Phys. Pol. B* **32** 871
- [12] Bogner S, Kuo T T S, Coraggio L, Covello A and Itaco N 2002 *Phys. Rev. C* **65** 051301(R)
- [13] Machleidt R 2001 *Phys. Rev. C* **63** 024001
- [14] Audi G, Wapstra A H and Thibault C 2003 *Nucl. Phys. A* **729** 337
- [15] Tanaka K *et al* 2010 *Phys. Rev. Lett.* **104** 062701
- [16] Ong H J *et al* 2008 *Phys. Rev. C* **78** 014308
- [17] Elekes Z *et al* 2009 *Phys. Rev. C* **79** 011302
- [18] Kemper K W and Cottle P D 2010 *Physics* **3** 13
- [19] Data extracted using the NNDC On-line Data Service from the ENSDF database, file revised as of June 4, 2010.
- [20] Hoffman C R *et al* 2009 *Phys. Lett. B* **672** 17
- [21] Coraggio L, Covello A, Gargano A and Itaco N 2009 *Phys. Rev. C* **80** 044311
- [22] Poves A, Nowacki F and Caurier E 2005 *Phys. Rev. C* **72** 047302
- [23] Coraggio L, Covello A, Gargano A, Itaco N and Kuo T T S 2008 *Nucl. Phys. A* **808** 424